Towards a thoracic conductive phantom for EIT

Serena de Gelidi[a,*], Nima Seifnaraghi[a], Andy Bardill[a], Yu Wu[b], Inéz Frerichs[c], Andreas Demosthenous[b], Andrew Tizzard[a], Richard Bayford[a]

[a] *Faculty of Science & Technology, Middlesex University, London, United Kingdom*
[b] *University College London, London, United Kingdom*
[c] *University Medical Centre Schlewig-Holstein, Kiel, Germany*

Number of words: 4854

Number of words in the abstract: 128

*Corresponding author
Email address: `s.degelidi@mdx.ac.uk` (Serena de Gelidi)

Abstract

Phantom experiments are a crucial step for testing new hardware or imaging algorithms for electrical impedance tomography (EIT) studies. However, constructing an accurate phantom for EIT research remains critical; some studies have attempted to model the skull and breasts, and even fewer, as yet, have considered the thorax. In this study, a critical comparison between the electrical properties (impedance) of three materials is undertaken: a polyurethane foam, a silicone mixture and a thermoplastic polyurethane filament. The latter was identified as the most promising material and adopted for the development of a flexible neonatal torso. The validation is performed by the EIT image reconstruction of the air filled cavities, which mimic the lung regions. The methodology is reproducible for the creation of any phantom that requires a slight flexibility.

Keywords: phantom, EIT, 3D printing, conductive, flexible

1. Introduction

Tissue-Mimicking Materials (TMM) are required to test and validate diverse emerging biomedical applications [1], including Electrical Impedance Tomography (EIT). EIT seeks to reconstruct the changes in impedance distribution within tissues caused by related physiological activities. This is achieved by acquiring data from injecting a set of currents into the body through surface electrodes and measuring the boundary voltages [2].

Definition

Phantoms are objects meant to replicate the main features of the final application of the device and associated anatomy under consideration. Phantom experiments are the bridge between computer-based simulations and clinical measurements, as they investigate the performance of the developed data-acquisition system, reconstruction algorithms or imaging software and subsequently provide reasonable information for further optimization [3]. Furthermore, phantoms allow a controlled *in vitro* testing, which is difficult to achieve in clinical experiments. A review of materials selected in previous works to generate a phantom is detailed in the following sections and summarised in Table 1.

The most common option

Saline-filled tanks, made of insulating materials and featuring metallic electrodes, are usually adopted to perform pilot measurements for EIT reconstructions [4, 5, 6]. Isaacson et al. [7] introduced anatomical features by suspending agar cross-sections of heart and lungs in a saline circular tank.

Flexible tanks and phantoms

Aiming to acquire boundary deformation measurements, Boyle et al. [8] designed a sponge rubber ring featuring stainless steel electrodes. As a result, the phantom was easy to compress yet its elasticity ensured the return to its original shape. Belmont et al. [9] showed that cylindrical tofu specimens were a viable phantom for soft TMM compression studies utilizing bioimpedance techniques. The main limitation of adopting food organic materials as TMM is their perishable nature. Despite the fact that several anthropomorphic resuscitation manikins are available to clinicians for training purposes, none of these can mimic the skin conductivity as they are made of insulating polymers. Since EIT can be adopted for different purposes, previous works have attempted the generation of an improved *in vitro* setup compared to the circular tanks. Tizzard et al. [10] used a gelatine breast phantom to ultimately generate a more accurate forward model. However, agar and gelatines degrade over time in contact with air or water, making them unsuitable for sporadic use over the long term [11].

Anatomically realistic phantoms

Recently, the idea of the common cylindrical tank has been upgraded into a geometrically accurate skull [11]. Hence, Avery et al. [11] 3D printed the skull model by means of a polylactic acid (PLA) filament and filled it with saline solution. As the adopted PLA is non conductive, they also needed to place 33 electrodes against the tank walls. Dunne et al. [12] employed a conductive material for generating the first anatomically accurate pelvic phantom for EIT. The chosen TMM was obtained by mixing the composition of 30% w/w graphite powder, 5.7% w/w carbon black (CB) powder and the remainder from equal parts of polyurethane precursors [1, 13]. A similar recipe was adopted to fabricate a two-layers head phantom for use in EIT [14] and breast tumours for Microwave Imaging [15]. Zhang et al. [3] created, based on 3D printing techniques, a novel four-layers structure head phantom with anatomically realistic geometry and continuously varying skull resistivity. Two types of acrylonitrile butadiene styrene (ABS) and CB particles with volume fractions of 10% and 20% CB were fabricated [3]. Similarly, Kurrant et al. [16] 3D printed a variety of sizes and shapes intended as breast models to test a prototype estimating the surface for Microwave Imaging. However, they did not specify the material used. Burfeindt et al. [17] prepared a 3D printed breast phantom made of ABS for use in microwave breast-imaging experiments. A different approach was attempted by Garrett and Fear [13], who created 3D printed molds to pour in a hand-made mixture of CB, graphite and rubber mixture [1]. Faenger et al. [18] were among the first to propose the application of conductive 3D printable filaments. Therefore, they claimed that conductive ABS or PLA are sensible choices. Their breast phantom for Microwave Imaging consisted in two interior 3D printed containers and a silicone composite based skin, which was created by mixing silicone, CB and graphite [18].

[Table 1 about here.]

Aim of the study

Therefore, the construction of an accurate phantom for EIT research remains a critical and challenging step. As part of the CRADL project (http://cradlproject.org/), which is developing EIT technology as supportive method for monitoring neonatal ventilation, the need of a phantom to test the prototypes arose. More generally, the phantom could help to improve the development of EIT and to establish it as a bedside method for optimising ventilation therapy [19]. The present study aims to develop a conductive and flexible neonatal phantom to test prototypes for the thoracic boundary detection [20] and EIT reconstruction. In order to generate a phantom, three materials have been selected and analysed in terms of both their electrical impedance properties and their production technique.

2. Materials and methods

2.1. Materials

The main requirements selected for developing the thoracic prototypes are the electrical conductivity and the elasticity, meaning that the mechanical behaviour of each material should feature low stiffness. Hence, three different materials have been selected to be compared:

A) A carbon impregnated polyurethane foam (Teknis Limited, UK).

B) A mix of a silicone (75%), CB powder (15%) and graphite powder (10%) [18], which needs to be synthesized. CB powder has been preferred over carbon fibres in order to promote the isotropy of the generated material.

C) A carbon filled thermoplastic polyurethane Palmiga 95-250 (Creative Tools, Sweden) has been acquired among the newest conductive and flexible filaments available for 3D printing.

2.2. Preparation

Five samples of each material were prepared, featuring the same cross-section (10mm x 10mm) and the following lengths: 10 mm, 20 mm, 30 mm, 40 mm and 50 mm. Different sample lengths were tested for linearity and homogeneity of the material, to record the variation in impedance. Successively, phantoms of idealized geometry were prepared in order to mimic the dimensions of a neonatal torso featuring a diameter of 7.5 cm and two lungs, simplified as through holes (Figure 1).

Material A is available in a ready to use form. However, since the foam is manufactured and sold in sheet form, it was cut by an abrasive water jet cutter.

Using similar methodology to Garrett and Fear [13], material B was prepared by hand in a fume hood due to the toxicity of CB in powder form. Hence, the rubber solution (prior to curing) was weighed and mixed in a container by hand. The CB powder was then weighed, added to the rubber mixture, and the materials were mixed with a metal stirrer for several minutes [1]. The mixture was prepared in accordance with the percentages reported by Garrett and Fear [1] to mimic the skin conductivity: 63 wt% silicone, 7 wt% CB, 30 wt% graphite. This choice is justified by the need to mimic a neonatal torso, in which the bone and the fat properties were assumed not to be overall predominant. However, the curing of the material B proved to be unsuccessful when using both a platinum-cure silicone Transil 20 (Mouldlife, UK) and a water white clear urethane Clear Flex 30 (Smooth-On, US). The same result was observed even when changing the percentages to the ones reported by Faenger et al. [18] for skin TMM: 75 wt% silicone, 15 wt% CB, 10 wt% graphite. However, such percentages were successfully adopted in the preparation of material B by the use of tin cure silicone TinSil Gel-10 (Polytek, US). Hence, powders were weighed and mixed. The two parts of the rubber solution were also weighed and mixed in a container by hand for a couple of minutes. Powders were added to the compound, which was stirred. In order to remove the majority of air bubbles the mixture was subjected to ultrasonication and then immediately poured in the custom-made mould.

Lastly, samples of the material C were 3D printed by means of a Printrbot Simple Metal (Printrbot, US). In order to obtain flexible samples, the infill was kept as low as 20%. Preliminary tests showed that printing below such value of infill led to suboptimal results. However, given the overall limited quality obtained and the fact that the other printers available were not compatible with such filament, the 3D print of the phantom was commissioned externally, keeping the same infill percentage.

[Figure 1 about here.]

2.3. Testing

Samples of each material were tested by means of a Solartron 1260 impedance analyzer (Solartron Analytical, UK) in order to compare their electrical properties. The absolute permittivity ϵ_{abs} has been measured by sweeping the frequency up to 2 MHz, which is the band of interest for biological tissues in the EIT field [21, 14]. The relative permittivity ϵ_r of each sample was calculated as: $\epsilon_r = \epsilon_{abs}/\epsilon_0$, where the vacuum permittivity ϵ_0 is approximated to $8.85 \cdot 10^{-12}$ $F \cdot m^{-1}$.

Following the characterization of the sample material, the contact impedance of each phantom was tested by means of an EIT setup. The system, shown in

Figure 2, mimics the EIT belt applied along the chest circumference of neonates as part of the CRADL project. The belt prototype was made of 32 copper tape electrodes placed on a PVC substrate. Salt-free electrode gel (Spectra 360, Parker Laboratories, US) was applied on the interface between the belt electrodes and the phantom. The raw measurements were recorded by the Pioneer Set (SenTec AG, CH) and processed in a Matlab (The MathWorks, US) custom script. The reference was taken by filling the holes of the model with cylinders of analogous electrical properties. In order to mimic the air content in the lungs, the main measurement featured the holes empty.

[Figure 2 about here.]

2.4. Image reconstruction

The idealized phantom model has been meshed in COMSOL Multiphysics (COMSOL Inc, SE) by means of 10,594 tetrahedral elements and exported to Matlab. Successively, the inverse model has been created by means of the GREIT algorithm [22] using the EIDORS v 3.9 toolbox (http://eidors3d.sourceforge.net/). The image is reconstructed using a difference EIT method [23] with the reference measurement, during which the through holes of the idealized phantom were filled by insertions made of the same material. Therefore, the reference domain is homogeneous.

2.5. The neonatal phantom

A thoracic model of a term baby, gestational age 38 weeks, has been previously developed based on the CT scans and ultrasound images [24]. Such a CAD model has been selected to create an anatomically accurate phantom of torso. The section between the shoulder height and the diaphragm has been chosen to identify clearly the armpit, as the anatomical landmark below which the EIT belt is usually placed by nurses. Hence, the CAD model has been cut, for the sake of practicality, parallel to the transverse plane. In addition, since the CRADL project focus is on lung ventilation, the model has been simplified by including only the lungs among the inner parts. The concavities of the lungs have been neglected in order to simplify the design. Lastly, the lungs have been designed as entities removable from the torso in order to mimic the air content by removing them prior to recording the reference data. Such a design forms the basis of further development of the phantom leading to more complex *in vitro* testing.

3. Results

3.1. Testing the samples

The average ϵ_r of the three materials, which was calculated after measuring the $\epsilon_{absolute}$ of each sample up to 2 MHz, is shown in Figure 3. The average ϵ_r of the 3D printed samples, made of material C, is always higher compared to the other materials. Materials A and B show the same permittivity above 100 KHz, while below such threshold the silicone B exhibits lower resistance to the electric field (Figure 3). The effect of the methodology adopted to prepare the samples is clearly reflected in the electrical properties: the hand-prepared mix leads to a high variability in the standard deviation, indicated by the blue error bars in Figure 3.

[Figure 3 about here.]

3.2. Testing the phantoms

The phantoms were tested by means of the EIT setup, shown in Figure 2, firstly without the use of electrode gel. The average contact impedances of all three materials were around 1460 Ω, being far too high for the application. This is motivated by the fact that the Pioneer Set has an impedance limit for the current source, defined as 700 Ω maximum. The application of the electrode gel on the interface lowered the contact impedance to 1100 Ω for material A, 1000 Ω for material B and 500 Ω for material C. Therefore, it was possible to carry out an EIT analysis only of the 3D printed phantom.

3.3. Image reconstruction

The EIT reconstruction of the 3D printed phantom was achieved by means of the GREIT algorithm [22]. As shown in Figure 4, the cavities were detected with the correct orientation in reference to the first electrode, which in EIDORS is represented in a lighter green compared to the others.

[Figure 4 about here.]

Given the results obtained, the neonatal phantom (Section 2.5) has been 3D printed by means of the material C, as shown in Figure 5, and tested similarly to the idealized one (Figure 2). The average contact impedance was 1410 Ω in absence of the electrode gel and lowered to 185 Ω when it was applied.

[Figure 5 about here.]

The measured voltages have been imported in Matlab in order to reconstruct the EIT image. The 3D geometry has been meshed in Comsol resulting in a model comprising 20,640 tetrahedral elements and 4483 nodes (Figure 6).

[Figure 6 about here.]

The blue areas shown in Figure 7 B highlight the detection of the lung cavities in the corresponding orientation reported in Figure 7 A.

[Figure 7 about here.]

4. Discussion

The present study has compared, for the first time, three materials for the preparation of a flexible and conductive phantom to be used for EIT *in vitro* testing. The sample preparation has highlighted the strengths and limitations of each material. The analysis below critically reviews each option. For example, material A has low elasticity and is therefore difficult to shape to the desired geometry by cutting. Moreover, as the material is only available in sheet form, larger phantoms would require many sheets to be laminated, presenting discontinuities in the model. Material B was obtained after attempting the polymerization with several silicones. The curing inhibition, which surprisingly has not been experienced in any previously reported work, could be related to impurities (e.g. sulphur) contained in the graphite. Therefore, it is suggested that the recipe used by Garrett and Fear [13], McDermott et al. [14] and Dunne et al. [12] may be polymerized only by using the specific polyurethane VytaFlex 20 (Smooth-On, US). In contrast to the foam, no limitation in terms of dimensions is associated with material B as long as a specific mould is prepared in advance. However, the manual preparation compromises the homogeneity of such a dense compound, which is reflected in the electrical properties (Figure 3). Although the recipe of Faenger et al. [18] allowed the preparation of the silicone mix and it was successfully used for Microwave Imaging, its resulting ϵ_r was about the same as that of the air in the tested frequency range (Figure 3). While the 3D printing process is extremely versatile, only selected printers can handle material C. Furthermore, the nozzle on the 3D printer can easily become clogged and adversely affected by the abrasive nature of carbon. Hence a hardened steel nozzle is commonly recommended.

Due to the contact impedance cut off of the Pioneer Set, materials A and B are deemed not viable for EIT purposes. This appears to be in contrast with Dunne et al. [12], however these authors reported a higher percentage of graphite for the pelvic phantom and they filled the cavity with sodium chloride and ultrasound gel.

The recorded values of contact impedance were 500 Ω and 185 Ω when electrode gel was applied to the 3D printed idealized and neonatal phantoms respectively. These values are close to the average of 300 Ω observed by Sophocleous et al. [25] in preterm infants after applying the neonatal ultrasound gel to the EIT belt (SenTec AG, CH) interface. Similarly, the median value of skin contact impedance observed in adults after applying the ContactAgent (SenTec AG, CH) on the textile EIT SensorBelt (SenTec AG, CH) was 325 Ω [26]. However, a wider range of contact impedances was recorded in this study compared to that undertaken by Sophocleous et al. [25]. The authors attribute such difference to the type of the electrodes, being textile in Sophocleous et al. [25] and made of simple copper tape in the present work.

Time-difference image reconstructions were successfully carried out using finite element models matching the experimental 3D printed phantom-prototype setup. Figures 4 and 7 show a change in conductivity in the correct location where the phantoms are air filled, respectively in the idealized and neonatal phantoms. Thus, it can be concluded that a carbon filled thermoplastic polyuretane phantom is a viable option for testing EIT prototypes. The additional advantages of such material are the possibility of generating a patient specific shape by using a 3D printer, as well as being flexible enough to emulate changes in lung shape over time.

Although the anatomical features for the neonatal torso and the human skull are different, this research confirms the accuracy in terms of location and shape of the target area detected as the electrical impedance imaging results are similar to the ones obtained by Zhang et al. [3], who generated and tested a 3D printed four-layer skull model made of ABS and CB. At present this article presents the first example of a neonate phantom for EIT. The use of a thermoplastic polyurethane increases the mechanical flexibility of the phantom, thus simulating the anatomical similarity. Unfortunately, mechanical properties of conductive filaments are rarely quantified by suppliers. According to the ISO 527, material C has an elongation at break of 250%, while carbon fibre ABS and PLA feature a value of 2% (CarbonX CF, 3DXTECH, US). Such ease of stretching of the selected material was modulated by the infill of the printing in order to mimic the torso flexibility.

Material homogeneity and the simplified internal design of the phantoms with the lungs being the sole internal components, represent the main limitations of the present work. In addition, even though the layer deposition of the printing process is consistent with the ribs' orientation and leads to an anisotropic behaviour of the phantom, this aspect is clearly simplified.

Overall, the material analysis carried out in this study will support the development of phantoms for other applications of EIT. In particular, the flexibility is a critical aspect to be replicated in several anatomically realistic applications, where a deformable boundary would lead to a different EIT image. The neonatal thorax is more compliant compared to the adult one by anatomical composition [27]. Future work will be undertaken to increase the complexity of the neonatal phantom, as the experimental evaluation of a prototype system is a necessary precursor to its clinical use. The authors aim to model different test scenarios, including diseased regions of the lungs.

5. Conclusion

Among the selection of materials and production techniques explored, the carbon filled thermoplastic polyuretane was favourably validated for the fabrication of an anatomically correct, conductive and flexible phantom. The 3D printing ensures the material homogeneity and the customization of the internal structure. A simplified neonatal torso of a phantom was thus generated. Similarly to the clinical practice, raw voltages were collected by means of the Pioneer set after applying a layer of ultrasound gel to the phantom surface. The corresponding image reconstruction showed the correct location of the air filled cavities, which feature a negative change of conductivity given the abovementioned material adopted for the phantom. The novel results obtained in this study are therefore highlighting the possibility to standardise the *in vitro* testing of the EIT device by using a known material before facing the huge biological variability of the clinical practice. Lastly, such phantom would be helpful to attempt different designs of belt without trying it on humans.

Acknowledgements

This work is supported by the CRADL project which has received funding from the European Unions Horizon 2020 research and innovation programme 2014-2018 under grant agreement No 668259.

Competing interests: None declared.

Ethical approval: Not required.

References

[1] J. Garrett, E. Fear, Stable and flexible materials to mimic the dielectric properties of human soft tissues, IEEE Antennas and Wireless Propagation Letters 13 (2014) 599–602. doi:10.1109/LAWP.2014.2312925.

[2] R. Bayford, Bioimpedance Tomography (Electrical Impedance Tomography), Annual Review of Biomedical Engineering 8 (2006) 63–91. URL: http://www.annualreviews.org/doi/10.1146/annurev.bioeng.8.061505.095716. doi:10.1146/annurev.bioeng.8.061505.095716.

[3] J. Zhang, B. Yang, H. Li, F. Fu, X. Shi, X. Dong, M. Dai, A novel 3D-printed head phantom with anatomically realistic geometry and continuously varying skull resistivity distribution for electrical impedance tomography, Scientific Reports 7 (2017) 4608. URL: http://www.nature.com/articles/s41598-017-05006-8. doi:10.1038/s41598-017-05006-8.

[4] A. P. Bagshaw, A. D. Liston, R. H. Bayford, A. Tizzard, A. P. Gibson, A. T. Tidswell, M. K. Sparkes, H. Dehghani, C. D. Binnie, D. S. Holder, Electrical impedance tomography of human brain function using reconstruction algorithms based on the finite element method, NeuroImage 20 (2003) 752–764. doi:10.1016/S1053-8119(03)00301-X.

[5] B. Grychtol, B. Müller, A. Adler, 3D EIT image reconstruction with GREIT., Physiological Measurement 37 (2016) 785–800. URL: http://www.ncbi.nlm.nih.gov/pubmed/27203184. doi:10.1088/0967-3334/37/6/785.

[6] C. Busch, B. Schullcke, K. Moeller, Realization of a multi-layer EIT-system, Current Directions in Biomedical Engineering 3 (2017) 291–294.

[7] D. Isaacson, J. L. Mueller, J. C. Newell, S. Siltanen, Reconstructions of chest phantoms by the D-bar method for electrical impedance tomography, IEEE Transactions on Medical Imaging 23 (2004) 821–828. doi:10.1109/TMI.2004.827482.

[8] A. Boyle, A. Adler, W. R. B. Lionheart, Shape Deformation in Two-Dimensional Electrical Impedance Tomography 31 (2012) 2185–2193.

[9] B. Belmont, R. E. Dodde, A. J. Shih, Impedance of tissue-mimicking phantom material under compression, Journal of Electrical Bioimpedance 4 (2013) 2–12. URL: https://www.journals.uio.no/index.php/bioimpedance/article/view/443. doi:10.5617/jeb.443.

[10] A. Tizzard, Borsic, R. Halter, R. H. Bayford, Generation and performance of patient-specific forward models for breast imaging with EIT, Journal of Physics: Conference Series 224 (2010) 012034. URL: http://stacks.iop.org/1742-6596/224/i=1/a=012034?key=crossref.39d32895f1b56224f9f42bee4635446a. doi:10.1088/1742-6596/224/1/012034.

[11] J. Avery, K. Aristovich, B. Low, D. Holder, Reproducible 3D printed head tanks for electrical impedance tomography with realistic shape and conductivity distribution, Physiological Measurement 38 (2017) 1116–1131. doi:10.1088/1361-6579/aa6586.

[12] E. Dunne, B. McGinley, M. O'Halloran, E. Porter, A realistic pelvic phantom for electrical impedance measurement, Physiological Measurement 39 (2018) 034001 (10pp). doi:https://doi.org/10.1088/1361-6579/aaa3c0.

[13] J. Garrett, E. Fear, A New Breast Phantom With a Durable Skin Layer for Microwave Breast Imaging, IEEE Transactions on Antennas and Propagation 63 (2015) 1693–1700. doi:10.1109/TAP.2015.2393854.

[14] B. McDermott, B. McGinley, K. Krukiewicz, B. Divilly, M. Jones, M. Biggs, M. O'Halloran, E. Porter, Stable tissue-mimicking materials and an anatomically realistic, adjustable head phantom for electrical impedance tomography, Biomedical Physics & Engineering Express 4 (2017) 015003. URL: http://stacks.iop.org/2057-1976/4/i=1/a=015003?key=crossref.5a638d936a7418d4d3f2a8c9b86e583b. doi:10.1088/2057-1976/aa922d.

[15] B. L. Oliveira, D. O'Loughlin, M. O'Halloran, E. Porter, M. Glavin, E. Jones, Microwave Breast Imaging: experimental tumour phantoms for the evaluation of new breast cancer diagnosis systems, Biomedical Physics & Engineering Express 4 (2018) 025036. URL: http://stacks.iop.org/2057-1976/4/i=2/a=025036?key=crossref.2405731769d3a91297cf3e51ebcb3394. doi:10.1088/2057-1976/aaaaff.

[16] D. Kurrant, J. Bourqui, E. Fear, Surface estimation for microwave imaging, Sensors (Switzerland) 17 (2017). doi:10.3390/s17071658.

[17] M. J. Burfeindt, T. J. Colgan, R. O. Mays, J. D. Shea, N. Behdad, B. D. Van Veen, S. C. Hagness, MRI-Derived 3-D-Printed Breast Phantom for Microwave Breast Imaging Validation, IEEE Antennas Wirel Propag Lett. 11 (2012) 1610–1613. doi:10.1016/j.jmb.2008.10.054.The. arXiv:NIHMS150003.

[18] B. Faenger, S. Ley, M. Helbig, J. Sachs, I. Hilger, Breast phantom with a conductive skin layer and conductive 3D-printed anatomical structures for microwave imaging, in: 11th EUCAP, volume 1, 2017, pp. 1065–1068. doi:10.23919/EuCAP.2017.7928662.

[19] I. Frerichs, M. B. P. Amato, A. H. van Kaam, D. G. Tingay, Z. Zhao, B. Grychtol, M. Bodenstein, H. Gagnon, S. H. Böhm, E. Teschner, O. Stenqvist, T. Mauri, V. Torsani, L. Camporota, A. Schibler, G. K. Wolf, D. Gommers, S. Leonhardt, A. Adler, Chest electrical impedance tomography examination, data analysis, terminology, clinical use and recommenda-

tions: consensus statement of the TRanslational EIT developmeNt stuDy group, Thorax 72 (2017) 83–93. doi:10.1136/thoraxjnl-2016-208357.

[20] S. de Gelidi, N. Seifnaraghi, A. Bardill, A. Tizzard, Y. Wu, E. Sorantin, S. Nordebo, A. Demosthenous, R. Bayford, Torso shape detection to improve lung monitoring, Physiological Measurement 39 (2018) 074001. URL: http://stacks.iop.org/0967-3334/39/i=7/a=074001?key=crossref.57a6cbf0eecc142bed13a34efc47650d. doi:10.1088/1361-6579/aacc1c.

[21] B. Rigaud, J.-P. Morucci, N. Chauveau, Bioelectrical impedance techniques in medicine Part I: Bioimpedance measurement second section: Impedance spectrometry, Critical Reviews in Biomedical Engineering (1997).

[22] A. Adler, J. H. Arnold, R. Bayford, A. Borsic, B. Brown, P. Dixon, T. J. Faes, I. Frerichs, H. Gagnon, Y. Gärber, B. Grychtol, G. Hahn, W. R. Lionheart, A. Malik, R. P. Patterson, J. Stocks, A. Tizzard, N. Weiler, G. K. Wolf, GREIT: A unified approach to 2D linear EIT reconstruction of lung images, Physiological Measurement (2009). doi:10.1088/0967-3334/30/6/S03.

[23] B. H. Brown, Electrical impedance tomography (EIT): A review, Journal of Medical Engineering and Technology 27 (2003) 97–108. doi:10.1080/0309190021000059687.

[24] N. Seifnaraghi, A. Tizzard, S. de Gelidi, D. Khodadad, S. Nordebo, A. H. van Kaam, I. Frerichs, A. Waldmann, E. Sorantin, S. Tschauner, A. Demosthenous, S. Christofides, R. Bayford, Estimation of Thorax Shape for Forward Modelling in Lungs EIT, in: A. Boyle, R. Halter, E. Murphy, A. Adler (Eds.), Proceeding of the 18th International Conference on Biomedical Applications of Electrical Impedance Tomography, Hanover (US), 2017, p. 58. doi:10.5281/zenodo.557093.

[25] L. Sophocleous, I. Frerichs, M. Miedema, M. Kallio, T. Papadouri, C. Karaoli, T. Becher, D. G. Tingay, A. H. Van Kaam, R. Bayford, A. D.

Waldmann, Clinical performance of a novel textile interface for neonatal chest electrical impedance tomography, Physiological Measurement 39 (2018). doi:10.1088/1361-6579/aab513.

[26] A. D. Waldmann, K. H. Wodack, A. März, A. Ukere, C. J. Trepte, S. H. Böhm, D. A. Reuter, Performance of Novel Patient Interface for Electrical Impedance Tomography Applications, Journal of Medical and Biological Engineering 37 (2017) 561–566. doi:10.1007/s40846-017-0264-y.

[27] A. Lander, J. Newman, Paediatric anatomy, Surgery 31 (2013) 101–105. URL: https://www.surgeryjournal.co.uk/article/S0263-9319(13)00003-3/pdf.

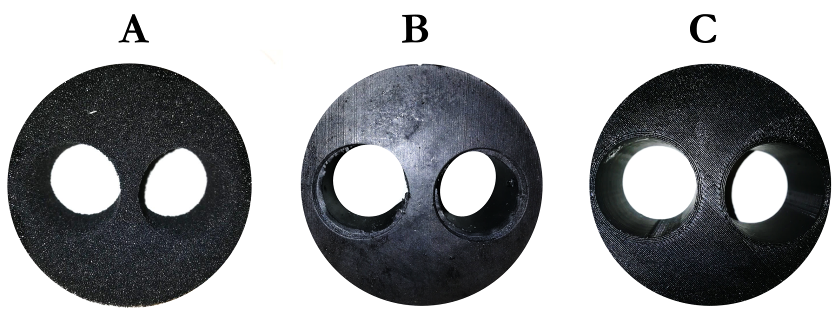

Figure 1: Phantoms of simplified and identical geometry to compare the material performance: A) carbon impregnated polyurethane foam; B) mix of a silicone in two parts, CB powder and graphite powder; C) 3D printed carbon filled thermoplastic polyurethane.

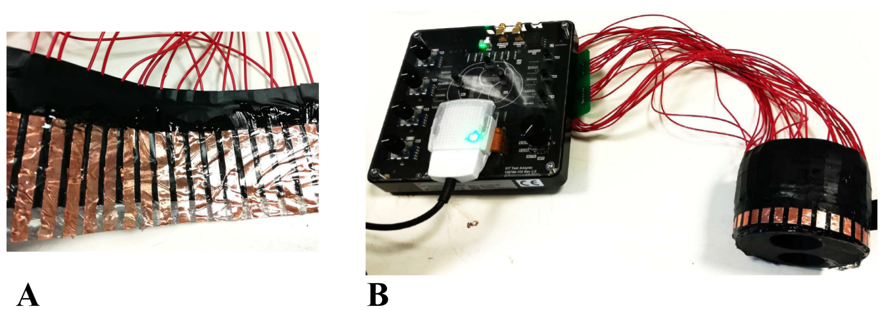

Figure 2: Testing the phantoms for EIT applications: A) Ultrasound gel applied on the interface between phantoms and 32-electrode belt; B) the belt is connected to the Pioneer Set, which records the raw voltages.

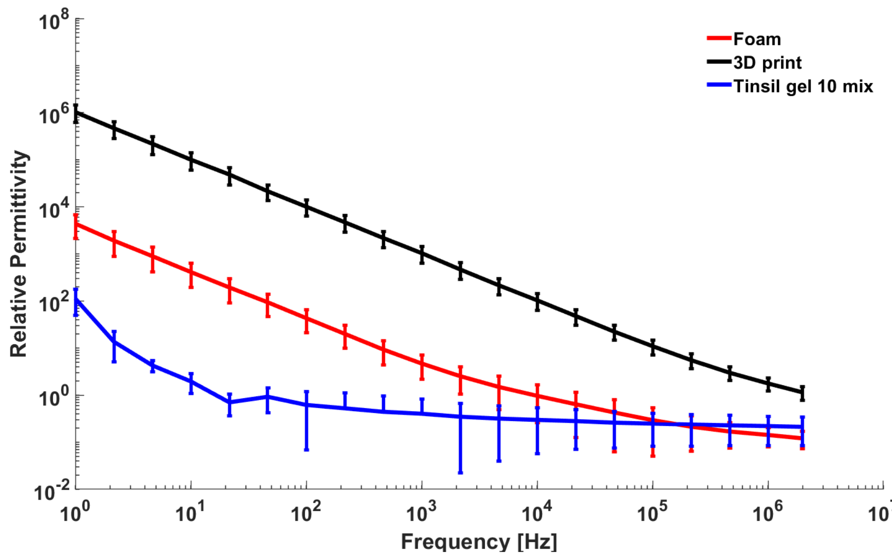

Figure 3: Mean relative permittivity (dimensionless) and standard deviation bars calculated for each sample of material tested by means of the impedance analyzer.

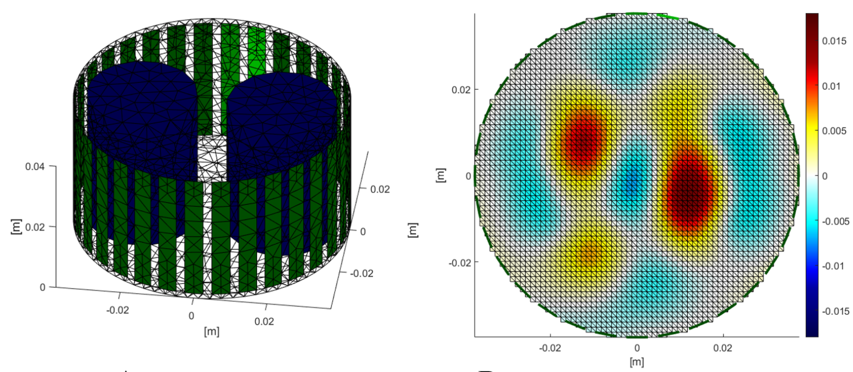

A **B**

Figure 4: EIT reconstruction of the 3D printed idealized phantom: A) Meshed geometry B) Image reconstruction.

A **B**

Figure 5: 3D printed phantom of neonatal torso (A) featuring removable lungs (B).

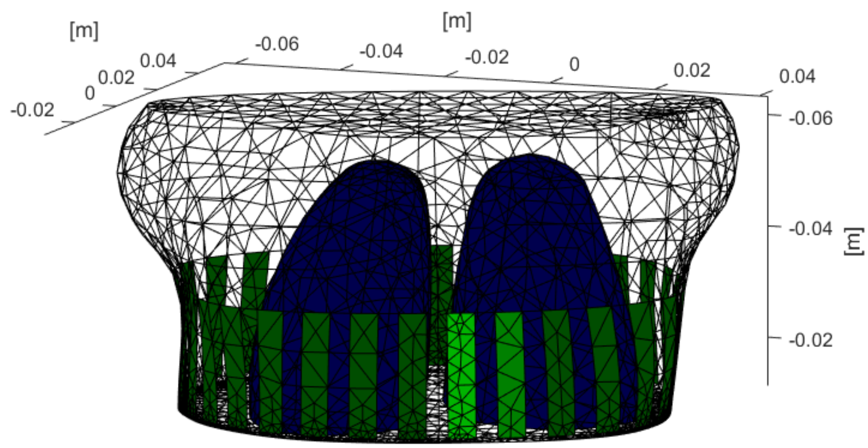

Figure 6: Neonatal phantom of torso meshed in Comsol and imported in the EIDORS toolbox.

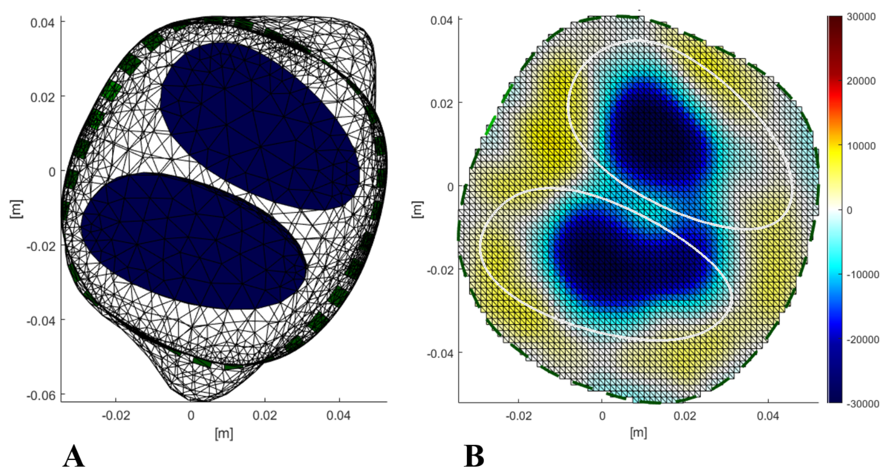

Figure 7: EIT analysis of the 3D printed neonatal phantom: A) Transverse view of the meshed geometry B) Image reconstruction.

Material	Conductive	Elastic*	Geometry	Adopted by
Sponge	No	Yes	Simplified	[8]
Tofu	Yes	No	Simplified	[9]
Agar	Yes	Depending on concentration	Simplified	[7, 10]
PLA	No	No	Anatomic	[11]
Mix of CB, graphite and silicone	Yes	Depending on concentration	Anatomic	[14, 18, 12, 15]
ABS and CB	Yes	No	Anatomic	[17, 18, 3]

Table 1: Literary review of materials used to generate phantoms. (*) Featuring low stiffness.